DC Islands in AC Smart Grids

Samuele Grillo, *Member, IEEE*, V. Musolino, Luigi Piegari, *Member, IEEE*, Enrico Tironi, and Carlo Tornelli

I. Introduction

NOWADAYS, distribution networks are changing substantially and rapidly. Environmental constraints, with particular attention to the reduction of CO_2, are leading the governments of major countries to use more and more renewable energy, particularly from wind and solar sources [1]–[4]. These sources are characterized by: 1) distribution in an area; 2) low power density for land occupation; and 3) discontinuity in power availability [5]. Moreover, power plants based on renewable energy are usually much smaller than traditional electrical generation plants, and the use of storage systems is advisable to benefit from the generation during low power demand periods and reduce alternative power flows along transmission lines, with consequent advantages in terms of system efficiency [5], [6].

This scenario is causing a change in distribution networks from passive to active grids, where the power flows, fault currents, and temporal power profile are quite different from the traditional ones [7]. Power injection on low voltage (LV) and medium voltage grids makes voltage regulation a difficult task. For this reason, different distribution system operators require mutual cooperation with the demand-side control because it is difficult to maintain the power quality using only supply-side control [8]–[10].

At the same time, the great evolution in informatics and telecommunications is leading the transformation of the traditional grids into smart grids, where the continuous dialogue between all of the devices connected to the network implies improvements in the overall efficiency and quality of the system. Moreover, it is also important to underline the wide diffusion of power electronic converters capable of decoupling the parameters (i.e., voltage and frequency) of the generators from the parameters of the network.

In this scenario, it could be convenient, in some cases, to substitute a dc grid for a traditional ac distribution network [11]–[13]. Indeed, a dc network, besides its well-known advantages with respect to ac systems [14], offers a simplification in relation to the power electronic converters for all of the devices operating on dc, i.e., photovoltaic (PV) systems and many storage systems. Moreover, it could eliminate all of the rectifiers present, as a first stage, in electrical drives and suppliers. For this reason, it is reasonable to imagine future smart grids realized using ac backbones and some dc leaves in the zones characterized by many small generation units, storage facilities, and users that are particularly susceptible to voltage disturbances. In such a network, it is possible to separate the backbones from the leaf regulation to ensure:

1) high power quality of the dc network;
2) management of power fluxes exchanged between the ac and dc sides with integrated ancillary services such as reactive power supply and harmonic compensation;
3) no increase in the fault currents even in the presence of new generation units;
4) the inhibition of disturbance propagation from the ac to dc side and vice-versa.

Starting from the aforementioned considerations, a dc test facility has been realized with the aim of verifying the potentiality of a dc island interconnected with an ac distribution network. The introduction of different power converters, especially those interfaced with different storage and renewable resources, requires a suitably designed management system in order to avoid uncontrolled power flows between the different elements. In order to realize a fully plug-and-play solution without a centralized management control unit, a methodology for designing the control loops of different converters based on traditional PI controllers is presented in next sections. This means that each converter works without exchanging information with the other units, and the insertion or disconnection of a single element from the dc network does not require a control system reconfiguration in order to guarantee the normal system operation. The main goals obtained through this methodology lie in:

Manuscript received October 19, 2012; revised January 15, 2013; accepted February 24, 2013. Date of current version July 18, 2013. Recommended for publication by Associate Editor P. C. Loh.

S. Grillo, L. Piegari, and E. Tironi are with the Dipartimento di Elettronica, Informazione e Bioingegneria, Politecnico di Milano, I-20131 Milan, Italy (e-mail: samuele.grillo@polimi.it; luigi.piegari@polimi.it; enrico.tironi@polimi.it).

V. Musolino is with the Dimac Red S.r.l, 20056 Biassono, Italy (e-mail: v.musolino@dimacred.it).

C. Tornelli is with the T&D technologies Department, RSE, 20134 Milan, Italy (e-mail: carlo.tornelli@rse-web.it).

Color versions of one or more of the figures in this paper are available online.

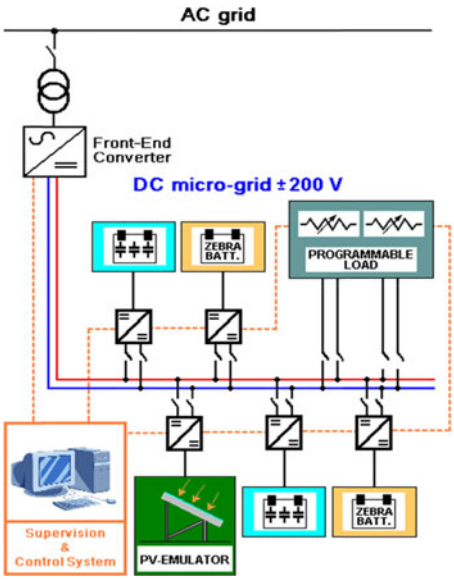

Fig. 1. Test facility configuration.

1) designing a dc network where different typologies of storage devices are connected in order to fulfill different system dynamic response performances;
2) designing disjoint control loop for each single power converter in order to avoid control overlapping;
3) designing the power converter control loops taking into account the behavior of the controlled device;
4) guaranteeing an embedded self-regulation of the state of charge (SoC) of the different storage devices.

In this way, this paper analyzes, besides the relevant aspects connected with the introduction in a smart grid of some dc islands to improve the power quality and energy efficiency of the system, the methodology to design a fully plug-and-play system solution without centralized communication infrastructure. The description of the test facility and its components is reported in Section II. In Section III, some case studies are described in order to demonstrate the advantage of the dc island introduction. In Section IV, the models of the components used for numerical simulations are discussed, while Section V proposes the methodology to set the control for each converter of the dc network. Finally, in Section VI, the results of numerical and experimental tests are reported and discussed.

II. Test Facility

The configuration of the test facility realized at RSE (the Italian Research Center on Energetic Systems) in collaboration with the Department of Electrical Engineering of the Politecnico di Milano is shown in Fig. 1.

The test facility was realized by taking into account the technical and economic constraints with the aim of studying the potentialities of LVDC active distribution networks, operated with suitable control strategies for the different devices connected to the network. The network has been equipped with different storage units in order to:

1) ensure the security for defined intervals of time when the ac grid is not available and the power generated on the dc network is insufficient to cover the power demand;
2) stabilize the dc voltage level if a sudden imbalance occurs between the power generated and consumed;
3) realize a peak shaving action in the presence of pulsing or intermittent loads, thus leveling the power drained by the ac grid;
4) implement an energy recovery action in the presence of regenerative loads;
5) realize the bridging and energy management functions that result from the presence of renewable sources.

In the following, a brief description of the main components of the test facility is given.

The LVDC microgrid has a voltage level of 400 V, and it is composed of a front-end ac/dc converter, energy storage elements, a PV field emulator, and controllable loads [15].

The front-end converter (FEC) has a rated power of 100 kW, which is a significant level compared with the maximum level to connect to an LV ac grid in several countries (Italy, Spain, Germany, and so on) [16]. This allows power flow in a case of insufficient or no generation, and also the opposite flow in the case of a generation surplus. The ac/dc FEC participates in the regulation of the dc network voltage and also detects the occurrence of an islanding condition by comparing the ac grid voltages and frequencies with their admissible ranges. The energy storage systems are composed of two ZEBRA batteries, each with a rated power of 32 kW, capacity of 64 Ah, and open-circuit voltage of 279 V, along with two supercapacitor banks, each made of no. 24 modules (30 kW for 4 s) with a maximum voltage of 384 V. Each ZEBRA battery and capacitor bank is coupled to the dc grid through a 35-kW dc/dc bidirectional converter to allow charging and discharging processes. In the following, the dc/dc converter interface between the ZEBRA batteries and dc bus will be indicated by the ZEBRA Converter (ZC), while the dc/dc converter connected to the supercapacitors will be indicated by the supercapacitor converter (SCC). The supercapacitor banks compensate for very fast fluctuations in the dc voltage caused by faults, dip propagation from the ac grid, or sudden load and/or generation changes in the dc grid. Because of the limited power from the PV fields available at the site as a result of both space constraints and meteorological conditions, a 35-kW PV field-emulator (PVC) has been chosen. In this way, the generated power can be controlled and the experimental activity is not constrained by weather conditions and daytime hours. Finally, two programmable purely resistive load-banks are installed in the dc microgrid; these two units can provide a total load of 60 kW. One bank, of 30 kW, can be regulated with step changes of 1 kW, while the other 30 kW bank is connected to the dc bus by means of a dc/dc converter for the fast regulation of the power absorbed.

III. Case Study

In order to test the capabilities of the dc network in achieving the above discussed goals, three kinds of cases were set and analyzed:

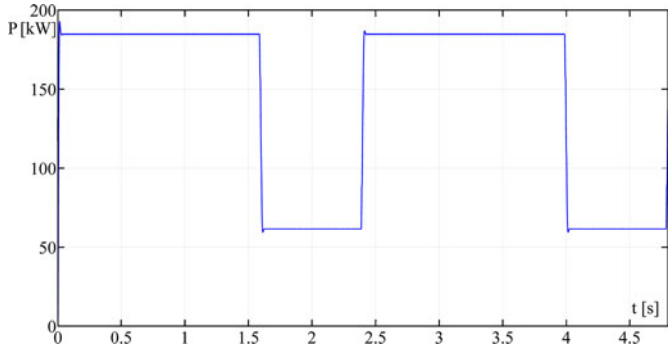

Fig. 2. Pulsing load simulating power profile of CAT.

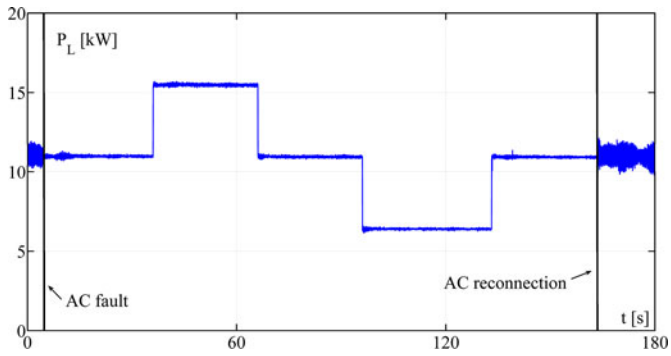

Fig. 3. Load power during ac network fault test.

1) pulsing load;
2) fault of the ac network while a step variable load is connected to the dc bus;
3) regenerative load.

A. Pulsing Load

A pulsing load is represented by a computer axial tomography (CAT) scanner, whose typical power diagram is a step load varying between about 60 and 180 kW with a period of 2.5 s and a duty cycle of 70%.

The power requested by this load is too high for the test facility. However, it can be scaled by taking into account the power of the different devices connected to the dc test facilities. Thus, the dc/dc converter connected 30-kW rated load has been programmed to absorb a power profile similar to that of a real CAT, although opportunely scaled. In Fig. 2, the power absorbed by the load during the tests is reported.

B. Fault in the AC Network

In the second test, an ac fault is simulated with the manual opening of the ac breaker connecting the FEC to the ac distribution network. The control algorithm of the converter detects the ac-side lack of voltage and disconnects the converter from the ac network. The simulated fault happens at time $t = 4.7$ s, while the ac reconnection is at $t = 163.5$ s. Meanwhile, the load demand changes with some steps simulating the connection and disconnection of different loads on the dc bus. In Fig. 3, the power profile of the experimental test is reported.

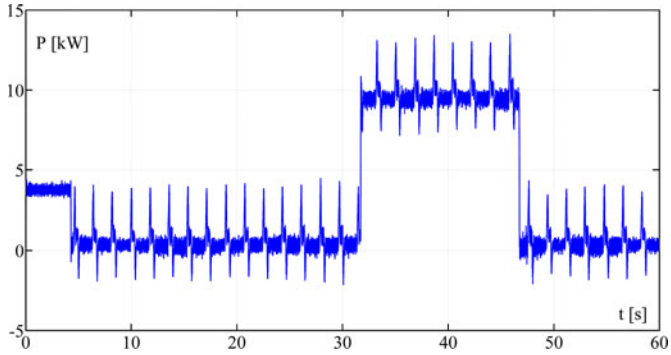

Fig. 4. Power diagram of simulated regenerative load.

C. Regenerative Load

Usually, electrical drives alternating between acceleration and braking operations are the most diffused regenerative loads. For this reason, the test to simulate regenerative loads is conducted by applying the real power demand of an electrical drive for a woodworking plant [17]. The working cycle lasts 1.9 s, with an acceleration phase (maximum power absorbed 3.5 kW), constant speed phase (power absorbed 700 W), and braking phase (maximum power regenerated 1.7 kW). The mean power absorbed during one cycle is lower than 200 W. Therefore, it is clear how the storage action of the dc system can lead to a significant energy recovery. Moreover, the insertion and disconnection of another load in parallel with the drive has been simulated. In particular, a 9-kW load is connected at time $t = 32$ s and disconnected at time $t = 47$ s. The experimental power diagram is reported in Fig. 4.

IV. Modeling of Electrical Storage

In order to correctly set up the control strategy for the different converters of the dc system, the modeling of the electrical storage devices is required. In particular, the ability of the model to represent the behavior of the electric storage over the full dynamic range of utilization is needed. The two operative working conditions of a storage device in grid applications are the following:

1) an energy function in which the device has to guarantee the average power requested by the application;
2) a peak shaving function in which the storage has to absorb/deliver the requested peak power above or below a certain reference average power.

In general, the first function is characterized by a significantly lower charge and discharge dynamic.

Among the various models available in the literature, we gave attention to lumped models capable of interpolating the device behavior as seen from the terminals.

A. ZEBRA Battery Model

The ZEBRA battery model comes from the lead acid battery dynamic models available in the literature [18]–[21]. In particular, in [18] and [19], lead acid battery models based on electrochemical impedance spectroscopy are described, while

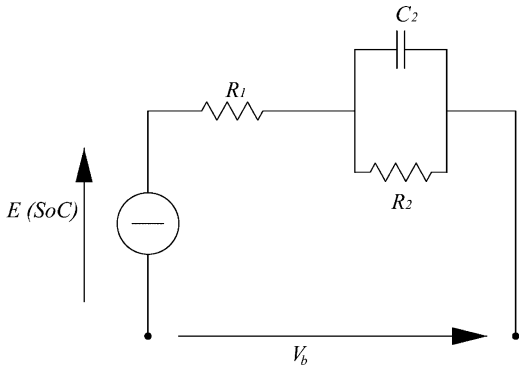

Fig. 5. ZEBRA battery model.

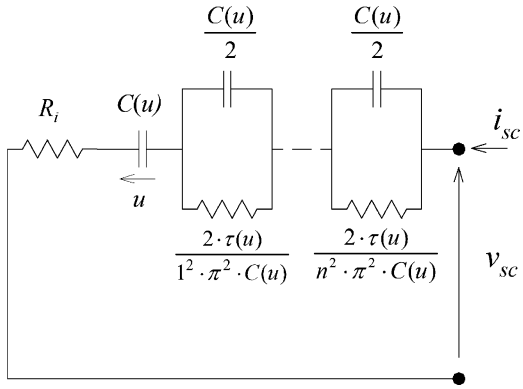

Fig. 6. Supercapacitor model.

in [20] and [21], third-order models that show a good compromise between complexity and precision are described.

The model used for our purpose is represented in Fig. 5 [22].

The ZEBRA battery is modeled as an electromotive force, *E(SoC)*, representing the open-circuit voltage as a function of the SoC, in series with the internal resistance, R_1, which takes into account the high-frequency resistance of the device, and the parallel branch, R_2C_2, which takes into account the dynamic behavior of the battery.

In addition, for our purpose, the battery temperature is considered to be constant during the work cycle, so that the equations describing the battery device are

$$E(SoC) = E_0 - K_e \cdot (1 - SoC) \tag{1}$$

$$SoC = 1 - \frac{1}{C_n} \int i_b \cdot dt \tag{2}$$

where E_0 is the open-circuit voltage when the battery is fully charged, *SoC* is the state of charge of the battery, C_n is the nominal battery capacity, K_e is a voltage constant, and i_b is the current supplied by the battery.

B. Supercapacitor Model

A supercapacitor model capable of representing the dynamics of the device in the typical frequency range of 10 mHz up to 100 Hz is represented in Fig. 6. This model, introduced in [23], was integrated in a more general model in [24], where a simplified procedure for the parameter identification was presented.

In this model, we have the following:

1) R_i represents the high-frequency resistance, which was available from the manufacturer's datasheet;
2) $C(u) = C_0 + K_V \times u$, where C_0 and K_V are constants evaluated by a constant current charge test, as described in [24];
3) $\tau(u) = 3 \times (R_{\rm dc} - R_i) \times C(u)$, where $R_{\rm dc}$ represents the dc resistance reported in the manufacturer's datasheet.

The supercapacitor and battery models used are unable to represent the redistribution and self-discharge of the devices. For our purposes, these phenomena, which take place at very low frequencies, almost close to dc, can be neglected without significant error.

V. Control Strategy

A control strategy for the network converters has been defined. In order to make the dc network capable of achieving all of the aims discussed in the previous sections, the control strategy should ensure:

1) the stabilization of the dc voltage during transients and at a steady state for different kind of loads;
2) the automatic configurability of the control scheme if one or more devices are unavailable;
3) the self-recharge of the storage systems;
4) the optimal utilization of all of the devices.

It is evident that to achieve the first goal, dc voltage control has to be implemented. However, there are four converters that can regulate the dc voltage: FEC, ZC, SCC, and PVC.

The possibility of splitting the voltage regulation requires the use of only one controller or of coordinated controllers. However, in order to realize a more robust control, it would be preferable to have separate controllers for the different units capable of working independently from the presence of the other units. The proposed control strategy is to design four control laws for the four converters. The control laws have to be adapted to the different devices they connect to the dc bus and have to be integrated in order to ensure both optimal working conditions for the different systems and high power quality on the dc bus. As will be shown in the next sections, these laws can be obtained using traditional control loops suitably tuned and modified. One of the innovative modifications consists in the self-recharge function that each storage system has to implement in order to keep, autonomously, its own SoC around the desired value. The tuning of the dynamic responses of the converters has to be coordinated to make each device work at its best and, at the same time, to guarantee the stabilization of the dc bus voltage. Thus, the dynamic response of each converter is tuned to optimally exploit the controlled device but it is also coordinated with the dynamic performances of the other converters. On the contrary, from an operation viewpoint, the controls of the four converters are independent from each other because they are based only on the measurement of voltage and current at their connection node.

The duty of imposing a stationary dc bus voltage can be assigned only to one converter; otherwise, the difference between the voltages measured at the different converters would

cause a continuous power flow from one converter to another, even in the absence of loads. The stiff voltage regulation has been committed to the FEC because the amount of energy in the ac network is consistently greater than the energy stored in the storage systems, and unlike the PV field, it is not dependent on weather conditions. The PVC implements a maximum power point tracking algorithm in order to draw the maximum possible energy from the PV field. It shuts down if a maximum voltage threshold is reached. Indeed, this happens only if the system is not able to absorb the energy produced by the PV field (i.e., if the ac network is not available and all of the storage systems are fully charged). The ZC and SCC contribute to voltage regulation but, in order to ensure stability, a droop control is implemented. In particular, in order to also perform the self-charging action, the droop is realized by taking into account the SoC. Thus, the voltage references for the ZC and SCC are dependent on the SoC values for the two storage systems, respectively. An optimal SoC has to be defined as a function of the goal of the network. For example, the optimal SoC for the batteries could be higher during the nighttime and lower during the daytime because the failure of the ac network during the daytime could be covered by the PV field, while the PVC cannot give energy to the loads during the nighttime.

In order to amplify the action of the supercapacitors when they are close to the optimal SoC, the SCC voltage reference is tuned to the supercapacitors' voltage instead of the supercapacitors' energy (proportional to the square of the voltage). In this way, their energy contribution is low when they are far from the optimal SoC.

In order to achieve the optimal use of the devices, it is also advisable that the power supplied by the FEC be the smoothest possible, feeding only the mean power request from the ac grid. Moreover, the supercapacitors should supply power during transients of a few seconds, while the batteries should work at time periods ranging from a few seconds to some minutes. The split of the power according to the dynamic performances of each device can be obtained based on the bandwidths of the converters' controllers. Indeed, the choice of different bandwidths implies different response times for the different devices.

As shown below, each converter is controlled by means of a feedback chain and PI regulator. In order to obtain the desired bandwidth for a power unit, it is necessary to choose suitable values for the regulator constants. It is, therefore, advisable to find the closed-loop transfer functions for the three power units.

A. Front-End Converter

The FEC is a traditional active front end. In order to control the FEC, a phase lock loop algorithm is implemented. After locking the grid phase, the control of the FEC operates on the rotating reference controlling the direct and quadrature components of the current [25]. Two nested feedback chains are implemented. The internal one uses the currents as inputs and the switching component control signals as outputs; the external one has the dc voltage and reactive power as inputs and the direct and quadrature currents as outputs. In relation to the dc voltage control, only the external chain is interesting. If the internal chain is much faster than the external one and is capable of setting the desired currents, the control scheme of the FEC can be drawn as reported in Fig. 7.

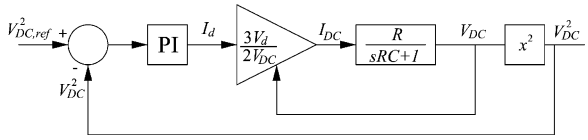

Fig. 7. Control scheme of FEC.

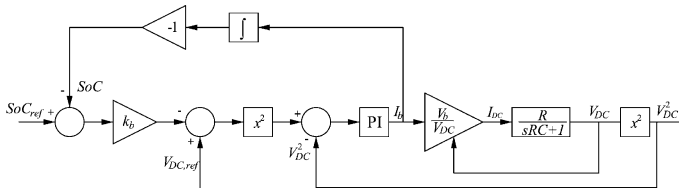

Fig. 8. Control scheme of ZC.

The closed-loop transfer function is

$$\frac{3\,V_d\;(k_p\,s+k_i)\,R}{2RC\,s^2+(3\,k_p\,V_d+2)\;s+3\,k_i\,V_d} \tag{3}$$

where V_d is the direct component of the grid voltage, k_p and k_i are the constants of the PI regulator, C is the total equivalent capacitance of the dc bus, and R is a resistive parameter representing the power absorbed by the dc bus.

As shown in Fig. 7, the feedback chain is realized on the square of the dc voltage. In this way, indeed, the tuning of the regulator is easier. In fact, in the frequency domain, the square of the dc voltage directly depends on the direct component of the grid current

$$\frac{V^2_{\mathrm{DC}}}{I_d}=\frac{3\,V_d}{2}\,\frac{R}{s\,RC+1}. \tag{4}$$

From (3), it is clear that the control system operates, globally, as a low-pass filter whose bandwidth limits the time response of the FEC.

B. ZEBRA Converter

The ZC is realized with one inverter leg acting as a bidirectional step-down/step-up converter. The high-voltage side is connected to the dc bus with an output capacitance, while the LV side is connected to the ZEBRA by means of an inductor. In addition, the ZC is operated with two nested feedback chains. The internal one controls the current in the inductance acting on the duty cycle of the switching components, while the external one regulates the dc voltage generating the reference current as an output. The control scheme of the external loop is reported in Fig. 8.

The self-recharge function is obtained changing the dc voltage reference in function of the SoC. This sort of droop action ensures that the battery tries to keep its SoC around the desired value. In any case, this action is slow if compared to the dynamic action of the control loop and can, therefore, be neglected in

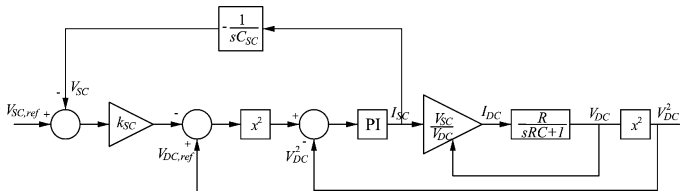

Fig. 9. Control scheme of SCC.

formulating the closed-loop transfer function

$$\frac{V_b\ (k_p\ s + k_i)\ R}{RC\ s^2 + (\ k_p\ V_b + 1)\ s + \ k_i\ V_b} \tag{5}$$

where V_b is the battery voltage.

C. Supercapacitors Converter

The SCC is realized using the same configuration as the ZC. The high-voltage side is connected to the dc bus with an output capacitance, while the LV side is connected to the supercapacitors by means of an inductor. In addition, the SCC is operated with two nested feedback chains. The internal chain controls the current in the inductance acting on the duty cycle of the switching components, while the external one regulates the dc voltage generating the reference current as an output. The control scheme of the external loop is reported in Fig. 9. It differs from the control scheme of the ZC in relation to the feedback on the supercapacitors' voltage.

The self-recharge function is obtained changing the dc voltage reference in function of supercapacitors voltage. This sort of droop action is introduced in order to keep the supercapacitors SoC around the desired value. Anyway, if k_{SC} is small enough, the action of the droop chain is slow if compared to the dynamic action of the control loop, and the closed-loop transfer function is

$$\frac{V_{\mathrm{SC}}\ (k_p\ s + k_i)\ R}{RC\ s^2 + (\ k_p\ V_{\mathrm{SC}} + 1)\ s + \ k_i\ V_{\mathrm{SC}}} \tag{6}$$

where V_{SC} is the supercapacitors' voltage.

VI. Numerical and Experimental Results

In order to test the proposed control strategy, many numerical and experimental tests have been performed. In the following, some results will be reported. In particular, these have been chosen to show how the same network, without changing the tuning of the controllers, can give very good results for the different applications discussed in Section III.

In order to achieve the required bandwidth separation of the controllers of the converters, the PI regulators have been tuned using the parameters reported in Table I. According to (3), (5), and (6), the speed response of the control answer depends on the load. For this reason, the bandwidths of the three converters change as a function of the power supplied to the dc bus, as reported in Fig. 10.

According to the bandwidths of the converters reported in Fig. 10, the action of the SCC will have a time constant of some hundreds of milliseconds, the ZC will act in seconds, while the intervention of the FEC will be slowed to tens of seconds. The constants k_b and k_{SC} are chosen taking into account the maximum desirable variation of the dc voltage and of the SoC of the two storage devices. In particular, for the batteries, considering a maximum allowable dc voltage variation of 10%, equal to 38 V, in correspondence of the chosen maximum depth of discharge (76%), it results $k_b = 0.5$. The desired SoC has been chosen equal to 90%. For what concerns the supercapacitors, the desired voltage value has been set to 220 V. Considering the possible voltage variation of 110 V (in fact half of the voltage corresponds approximately to three-fourth of the stored energy) and associating it to an admissible dc voltage variation of 4%, it results $k_{\mathrm{SC}} = 1/7$. It is worth noting that the admissible dc voltage variation for the SCC has been chosen lower than that of the ZC. This is the reason why the supercapacitors action is expected to be quicker than that of the batteries.

In the following, the results obtained by applying the three loads presented in Section III are analyzed.

In particular, three cases have been numerically simulated and experimentally tested. All of these tests lasted 3 min. They are summarized in Table II and reported as follows:

TABLE I
Parameters of Converter Regulators

FEC		ZC				SC			
k_p	k_i	k_p	k_i	k_b	SOC_{ref} [%]	k_p	k_i	k_{SC}	$V_{SC,ref}$ [V]
0.001	0.002	0.005	0.01	0.5	90	0.01	0.1	0.143	220

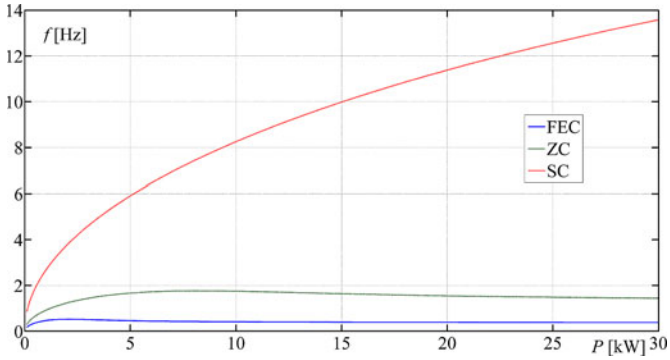

Fig. 10. Bandwidths versus power of three converters.

TABLE II
Test Cases Analyzed in the Paper

Case study	Key features	Notes
Pulsing load	P_{max} = 19 kW, P_{min} = 8 kW T = 2.5 s, duty cycle = 66%	AC grid is disconnected from t = 1 s to t = 2 s. Disconnection and reconnection times are lagged in experimental test
Fault of AC network	P_{max} = 4.5 kW, P_{min} = -4.5 kW $T_{disconn.}$ = 4.7 s, $T_{reconn.}$ = 163.5 s step variations of DC loads	
Regenerative load	P_{max} =3.5 kW, P_{min} = –1.7 kW P_{mean} = 200 W	a 9 kW load is connected from t = 32 s to t = 47 s

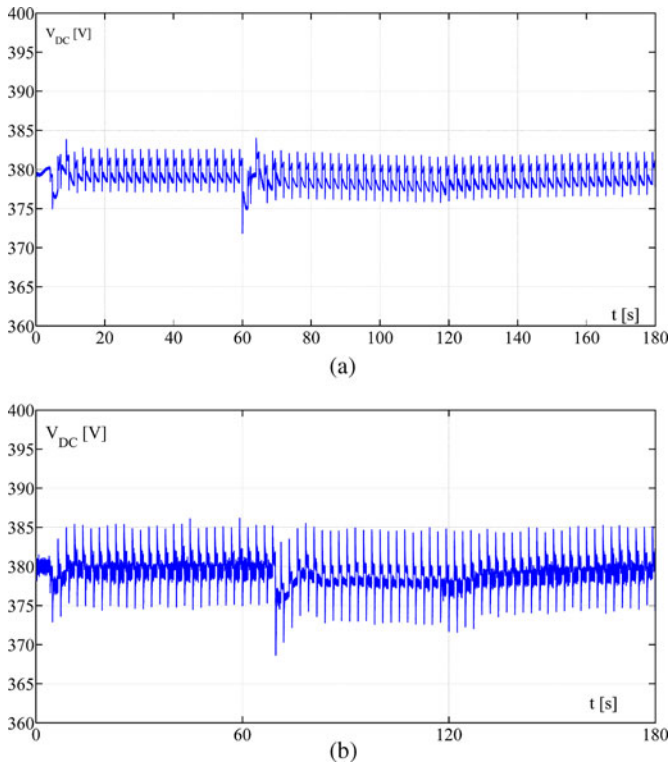

Fig. 11. DC voltages. (a) simulated. (b) measured.

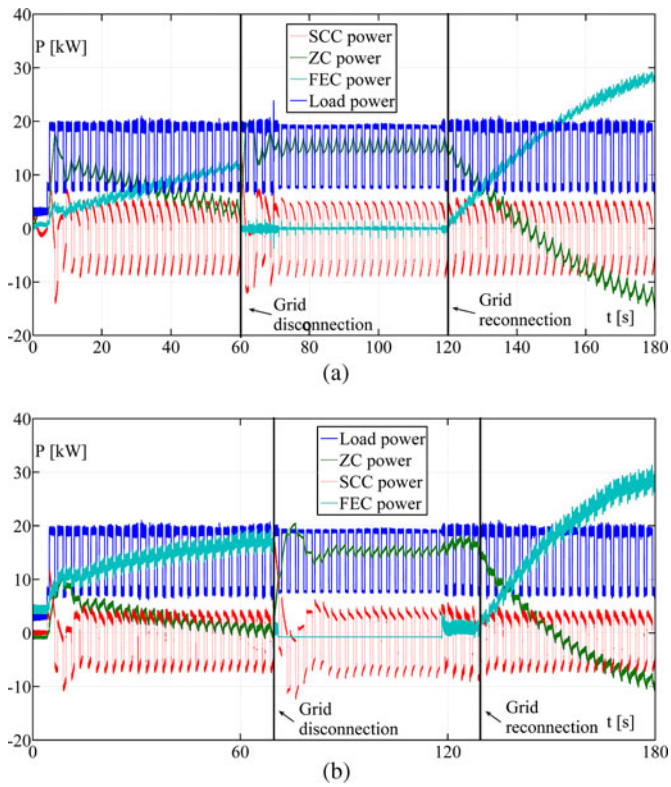

Fig. 12. Power supplied by different devices. (a) simulated. (b) measured.

1) In the first test, the pulsing load of Fig. 2 is applied to the system. A disconnection of the ac grid is simulated between about 1 and 2 min.
2) In the second test, the response of the system to the power request reported in Fig. 3 is performed. In this case, a network failure occurs at the first instant and almost lasts for all 3 min.
3) In the third test, the regenerative load of Fig. 4 is applied to the system. A step load variation occurs between $t_1 = 32$ s and $t_2 = 46$ s.

In the following, the results obtained in numerical simulations and experimental tests are reported and discussed.

A. Pulsing Loads

The pulsing load of Fig. 2 is applied to the system. In order to develop the numerical simulations, the measured power requested by the load is used in simulating the load behavior. The test lasts 3 min, during which a disconnection of the ac grid is simulated between about 1 and 2 min. In Fig. 11(a) and (b), the simulated and experimental dc voltages are reported.

The voltage excursion is very limited ($\pm 2\%$), and when the ac grid is disconnected, the voltage drop is lower than 3%. The power supplied by each device is reported in Fig. 12. The experimental results match those obtained in the numerical simulations.

Even if a centralized control action is not implemented, the different converters are able to split the load power diagram adapting it to the characteristics of the different devices. Indeed, as is clear from Fig. 12, the pulsing power is supplied essentially by the SCC because of its higher bandwidth. The FEC, presenting the lower bandwidth, supplies only the mean power. At the grid disconnection, in the first instants, the SCC supplies the whole load demand. After some seconds, as allowed by its bandwidth, the ZC supplies the mean power and also recharges the supercapacitors.

At the grid reconnection, the ZC automatically drains energy from the dc bus to recharge the batteries. This is the reason why the FEC supplies a power greater than the load power request. This self-recharge action is obtained by the droop action introduced in the control of the ZC and shown in Fig. 8. Indeed, during the main grid disconnection, the batteries have been discharged and their dc reference has been decreased. The difference between the rated value of the dc reference and the dc reference of the ZC is the cause of the recharging process occurring at the network reconnection. When the SoC of the batteries reaches the desired value, the two dc references are equal and the self-recharge ends. Similarly, the supercapacitors keep their voltage around the desired value of 220 V. Fig. 13 shows the ability of the SCC to keep the desired value of the supercapacitors' SoC.

B. Fault of the AC Network

In order to show the ability of the system to ensure a high-quality energy supply even when a main grid faults occurs, the load condition presented in Fig. 3 is numerically simulated and experimentally realized. In Fig. 14, the dc voltage is reported.

The voltage fluctuation around the rated value of 380 V is caused by the changing SoC of the batteries. While the batteries change their SoC absorbing from or supplying power to the

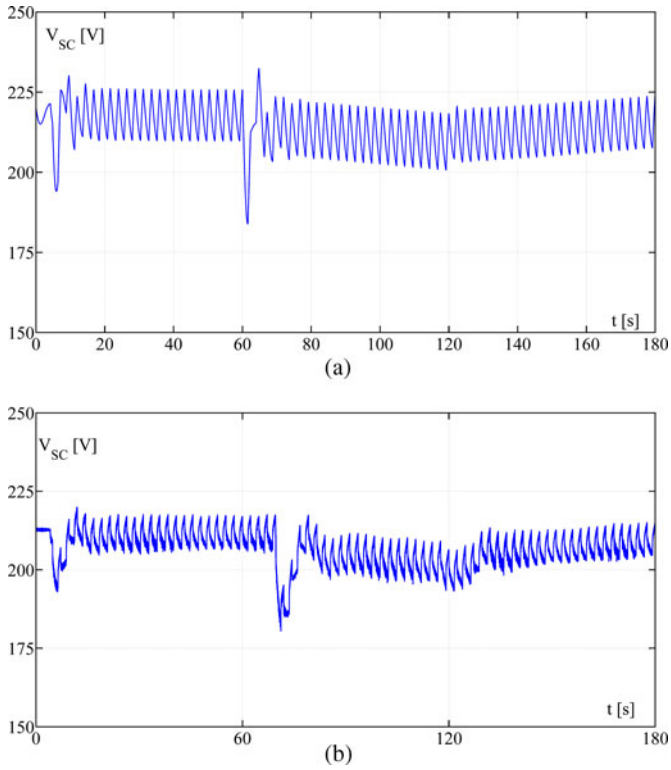

Fig. 13. Supercapacitors' voltages. (a) simulated. (b) measured.

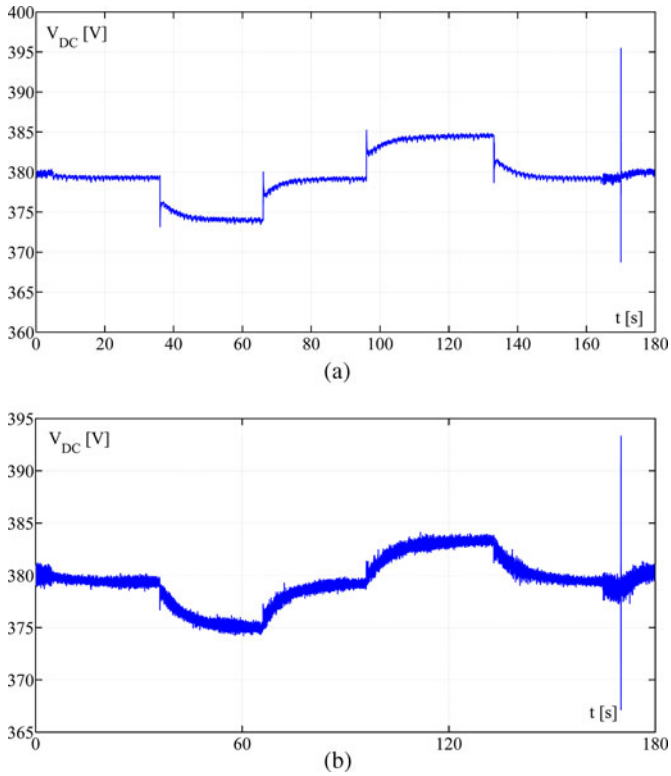

Fig. 14. DC voltage. (a) simulated. (b) measured.

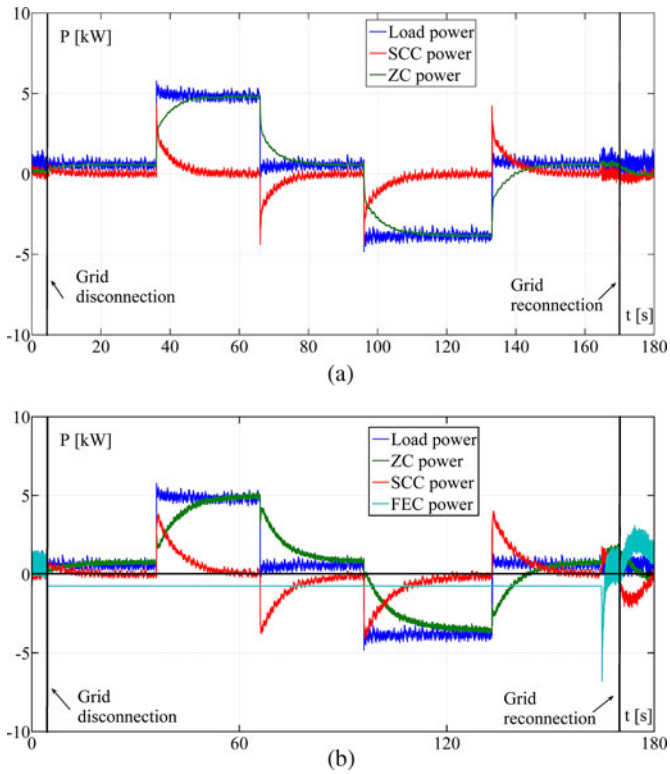

Fig. 15. Simulated power supplied by different devices. (a) simulated. (b) measured.

load, their dc voltage reference is changed by the droop action necessary to realize the self-recharge action.

However, the choice of a low value for k_b ensures that the dc voltage is always inside a very tight band.

The powers exchanged between the dc bus and the different devices are reported in Fig. 15.

For the different bandwidths of the controllers, at each power change, the first device to take action is the SCC. It is worth noting that during the absence of the ac grid, the FEC is a load because it supplies its auxiliaries by drawing power from the dc bus.

C. *Regenerative Loads*

Finally, the case of a regenerative load is numerically simulated and experimentally tested. In this case, no large amount of energy is exchanged and, for this reason, the predominant action of the supercapacitors is advisable. This is realized by the higher bandwidth of the SCC that makes it work as the main *power source*. In Fig. 16, the dc bus voltage is reported.

In Fig. 17, the powers supplied by each device are reported. It is clear that the alternative power demand is covered essentially by the supercapacitors because it occurs in times lower than 1 s where the predominant answer is that of the SCC (see Fig. 10). In addition, during the transient associated with the load step variation (at time $t = 32$ s), the SCC keeps supplying the alternative power beyond the contribution to the transient power request.

It is worth noting that the ZC drains power from the dc bus before the time instant of 32 s because the SoC of the batteries is lower than the reference one.

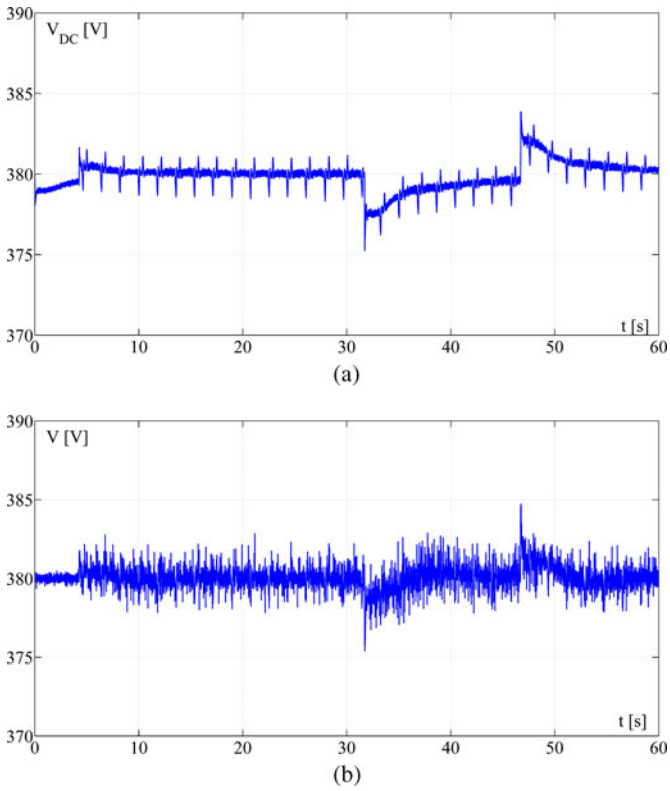

Fig. 16. DC voltages. (a) simulated. (b) measured.

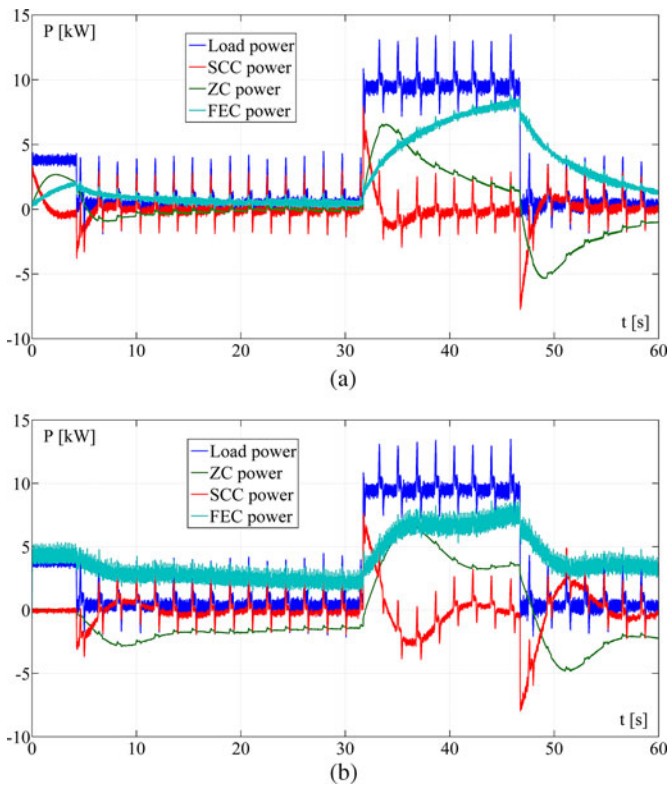

Fig. 17. Power supplied by different devices. (a) simulated. (b) measured.

VII. Conclusion

The wide diffusion of distributed renewable energy sources connected to distribution networks presents a new scenario for the regulation of distribution networks. Moreover, the availability of new technologies for storage systems encourages their use in power systems to achieve the goals of voltage stabilization and regulation, continuity of service, peak shaving, and the matching of generated and requested power profiles. In this scenario, the use of dc microgrids, connected as leaves to an ac backbone, is an effective possibility to obtain a high-quality distribution network. Indeed, a dc microgrid not only allows the easier connection of renewable sources and storage systems, but also makes it possible to eliminate all of the input rectifiers installed inside electrical drives and suppliers. Thus, the advantages of using a hybrid ac+dc distribution system involve not only the quality of the service but also the efficiency of the overall system.

In order to conduct some preliminary experiments on this kind of distribution scheme, a 100-kW dc test facility has been realized at RSE, Milan, Italy. This facility has been used to set up a control strategy for all of the converters interconnecting devices to a dc bus (ac network, generation unit, storage systems, and loads).

In this paper, after a description of the test facility, a robust control strategy has been proposed to show the capabilities of a dc microgrid in terms of the continuity of the service, power quality level, and energy saving. The proposed control strategy does not need a central intelligence, because each converter control acts only on the basis of the dc bus voltage. In order to set up the proposed strategy, preliminary numerical simulations were performed after modeling all of the devices connected to the network. Then, some experimental tests were carried out in order to verify that all of the requested goals had been achieved. The reported experimental results showed the continuity of service when a fault occurred on the ac grid, and voltage stabilization and regenerative actions were effectively performed by the dc microgrid. Moreover, the control of the converters allowed the decoupling of the dynamic responses of the different units, making each device work at its best potential. Finally, the self-recharging of the storage systems was integrated into the control logic and was effectively achieved, as shown by the experimental results.

References

[1] N. Hadjsaid, R. Caire, and B. Raison, "Decentralized operating modes for electrical distribution systems with distributed energy resources," in *Proc. IEEE Power Energy Soc. General Meeting*, Jul. 26–30, 2009, pp. 1–4.

[2] A. Soni and C. S. Ozveren, "Renewable energy market potential in U.K," in *Proc. 42nd Int. Univ. Power Eng. Conf.*, Sep. 4–6, 2007, pp. 717–720.

[3] Y.-w. Song, "American policy on renewable energy and its inspiration," in *Proc. Int. Conf. Manag. Sci. Eng.*, Nov. 24–26, 2010, pp. 1513–1519.

[4] P. Sarikprueck, S. K. Korkua, W.-J. Lee, and P. Lumyong, "Developing important renewable energies in Thailand," in *Proc. IEEE Power Energy Soc. General Meeting*, Jul. 24–29, 2011, pp. 1–8.

[5] J. M. Carrasco, L. G. Franquelo, J. T. Bialasiewicz, E. Galvan, R. C. P. Guisado, M. A. M. Prats, J. I. Leon, and N. Moreno-Alfonso, "Power-electronic systems for the grid integration of renewable energy sources: A survey," *IEEE Trans. Ind. Electron.*, vol. 53, no. 4, pp. 1002–1016, Jun. 2006.

[6] M. D. Hopkins, A. Pahwa, and T. Easton, "Intelligent dispatch for distributed renewable resources," *IEEE Trans. Smart Grid*, vol. 3, no. 2, pp. 1047–1054, Jun. 2012.

[7] X. Mamo, S. Mallet, T. Coste, and S. Grenard, "Distribution automation: The cornerstone for smart grid development strategy," in *Proc. IEEE Power Energy Soc. General Meeting*, Jul. 26–30, 2009, pp. 1–6.

[8] *Standard for Interconnecting Distributed Resources with Electric Power Systems*, IEEE Standard 1547, 2003.

[9] *Reference technical rules for the connection of active and passive consumers to the HV and MV electrical networks of distribution Company*, CEI 0-16 fasc. 9251, 2008.

[10] *Reference technical rules for the connection of active and passive users to the LV electrical Utilities*, CEI 0-21 fasc. 11666, 2011.

[11] M. E. Baran and N. R. Mahajan, "DC distribution for industrial systems: Opportunities and challenges," *IEEE Trans. Ind. Appl.*, vol. 39, no. 6, pp. 1596–1601, Nov./Dec. 2003.

[12] A. Kwasinski and C. N. Onwuchekwa, "Dynamic behavior and stabilization of DC microgrids with instantaneous constant-power loads," *IEEE Trans. Power Electron.*, vol. 26, no. 3, pp. 822–834, Mar. 2011.

[13] J. Lago and M. L. Heldwein, "Operation and control-oriented modeling of a power converter for current balancing and stability improvement of DC active distribution networks," *IEEE Trans. Power Electron.*, vol. 26, no. 3, pp. 877–885, Mar. 2011.

[14] C. D. Xu and K. W. E. Cheng, "A survey of distributed power system—AC versus DC distributed power system," in *Proc. 4th Int. Conf. Power Electron. Syst. Appl.*, Jun. 8–10, 2011, pp. 1–12.

[15] V. Musolino, L. Piegari, E. Tironi, L. Martini, A. Brambilla, and C. Tornelli, "Simulations and field test results for potential applications of LV DC distribution network to reduce flicker effect," in *Proc. 14th Int. Conf. Harmonics Quality Power*, Sep. 26–29, 2010, pp. 1–6.

[16] I. Stadler, "Study about International Standards for the connection of Small Distributed Generators to the power grid," [Online]. Available: http://www.americadosol.org/wp-content/uploads/2011/07/International-Standards-for-the-connection-of-Small-Distri.-Generators-Cologne-University-GIZ-2011.pdf

[17] V. Musolino, L. Piegari, Tironi, C. Tornelli, and A. Villa, "High power quality level DC distribution system for woodworking plants," in *Proc. 15th Int. Conf. Harmonics Quality Power*, Jun. 2012, pp. 1–7.

[18] P. Mauracher and E. Karden, "Dynamic modelling of lead/acid batteries using impedance spectroscopy for parameter identification," *ELSEVIER J. Power Sources*, vol. 67, pp. 69–84, 1997.

[19] H. Andersson, I. Petersson, and E. Ahlberg, "Modelling electrochemical impedance data for semi-bipolar lead acid batteries," *J. Appl. Electrochem.*, vol. 31, pp. 1–11, 2001.

[20] N. Moubayed, J. Kouta, A. EI-AIi, H. Dernayka, and R. Outbib, "Parameter identification of the lead acid battery model," in *Proc. 33rd IEEE Photovoltaic Spec. Conf.*, 2008, pp. 1–6.

[21] M. Ceraolo, "New dynamical models of lead acid batteries," *IEEE Trans. Power Syst.*, vol. 15, no. 4, pp. 1184–1190, Nov. 2000.

[22] M. Einhorn, F. V. Conte, C. Kral, and J. Fleig, "Comparison, selection, and parameterization of electrical battery models for automotive applications," *IEEE Trans. Power Electron.*, vol. 28, no. 3, pp. 1429–1437, Mar. 2013.

[23] S. Buller, E. Karden, D. Kok, and R. W. De Doncker, "Modeling the dynamic behavior of supercapacitors using impedance spectroscopy," *Ind. Appl. Conf.*, vol. 4, pp. 2500–2504, 2001.

[24] V. Musolino, L. Piegari, and E. Tironi, "New full-frequency-range supercapacitor model with easy identification procedure," *IEEE Trans. Ind. Electron.*, vol. 60, no. 1, pp. 112–120, Jan. 2013.

[25] L. Piegari and P. Tricoli, "A control algorithm of power converters in smart-grids for providing uninterruptible ancillary services," in *Proc. 14th Int. Conf. Harmonics Quality Power*, Sep. 26–29, 2010, pp. 1–7.